Single-step detection of norovirus tuning localized surface plasmon resonance-induced optical signal between gold nanoparticles and quantum dots

Single-step detection of norovirus tuning localized surface plasmon resonance-induced optical signal between gold nanoparticles and quantum dots

Fahmida Nasrin[a], Ankan Dutta Chowdhury[b], Kenshin Takemura[a], Jaewook Lee[b], Oluwasesan Adegoke[b], Vipin Kumar Deo[c], Fuyuki Abe[d], Tetsuro Suzuki[e], Enoch Y. Park[*,a,b]

[a] *Laboratory of Biotechnology, Graduate School of Science and Technology, Shizuoka University, 836 Ohya, Suruga-ku, Shizuoka 422-8529, Japan*

[b] *Laboratory of Biotechnology, Research Institute of Green Science and Technology, Shizuoka University, 836 Ohya, Suruga-ku, Shizuoka 422-8529, Japan*

[c] *Organization for International Collaboration, Shizuoka University, 836 Ohya, Suruga-ku, Shizuoka 422-8529, Japan*

[d] *Department of Microbiology, Shizuoka Institute of Environment and Hygiene, 4-27-2, Kita-ando, Aoi-ku, Shizuoka 420-8637, Japan*

[e] *Department of Infectious Diseases, Hamamatsu University School of Medicine, 1-20-1 Higashi-ku, Handa-yama, Hamamatsu 431-3192, Japan*

E-mails:

fnsoma@yahoo.com (FN)
dc_ankan@yahoo.co.in (ADC)
takemura.kenshin.16@shizuoka.ac.jp (KT)
lee.jaewook@shizuoka.ac.jp (JL)
adegoke.sesan@mailbox.co.za (OA)
deo.vipin.kumar@shizuoka.ac.jp (VKD)
fuyuki1_abe@pref.shizuoka.lg.jp (FA)
tesuzuki@hama-med.ac.jp (TS)
park.enoch@shizuoka.ac.jp (EYP)

[*] Corresponding author at: Research Institute of Green Science and Technology, Shizuoka University, 836 Ohya, Suruga-ku, Shizuoka 422-8529, Japan.
E-mail address: park.enoch@shizuoka.ac.jp (E.Y. Park). Tel (Fax): +81-54-238-4887)

Abstract

A new method of label free sensing approach with superior selectivity and sensitivity towards virus detection is presented here, employing the localized surface plasmon resonance (LSPR) behavior of gold nanoparticles (AuNPs) and fluorescent CdSeTeS quantum dots (QDs). Inorganic quaternary alloyed CdSeTeS QDs were capped with L-cysteine via a ligand exchange reaction. Alternatively, citrate stabilized AuNPs were functionalized with 11-mercaptoundecanoic acid to generate carboxylic group on the gold surface. The carboxylic group on the AuNPs was subjected to bind covalently with the amine group of L-cysteine capped CdSeTeS QDs to form CdSeTeS QDs/AuNPs nanocomposites. The fluorescence of CdSeTeS QDs/AuNPs nanocomposite shows quenched spectrum of CdSeTeS QDs at 640 nm due to the close interaction with AuNPs. However, after successive addition of norovirus-like particles (NoV-LPs), steric hindrance-induced LSPR signal from the adjacent AuNPs triggered the fluorescence enhancement of QDs in proportion to the concentration of the target NoV-LPs. A linear range of 10^{-14} to 10^{-9} g mL^{-1} NoV-LPs with a detection limit of 12.1 $\times$ 10^{-15} g mL^{-1} was obtained. This method was further applied on clinically isolated norovirus detection, in the range of 10^{2} – 10^{5} copies mL^{-1} with a detection limit of 95.0 copies mL^{-1}, which is 100-fold higher than commercial ELISA kit. The superiority of the proposed sensor over other conventional sensors is found in its ultrasensitive detectability at low virus concentration even in clinically isolated samples. This proposed detection method can pave an avenue for the development of high performance and robust sensing probes for detection of virus in biomedical applications.

Keywords: Biosensor; CdSeTeS; Gold nanoparticle; Localized surface plasmon resonance; Norovirus detection; Quantum dots.

1. Introduction

The current progress in search of optically active nanocomposite has driven the development of variety of applications in diverse fields ranging from biomedical engineering to environmental safety (Dutta Chowdhury and Doong, 2016; Ganganboina et al., 2017; Hsu et al., 2016; Kuila et al., 2011; Lee et al., 2007). Although several developments of optical biosensors have been experienced an exponential growth during the last decade due to the incorporation of nanotechnology for the direct, real-time and label-free detection of many chemical and biological substances (Anh et al., 2017; Chowdhury et al., 2012; Dutta Chowdhury et al., 2017), but there are very few reports which come to appear in real applications. Fluorometric assays are the most often applied methods on optical sensing and comes in a variety of schemes due to its easy technique and reliable outcomes (Al-Ogaidi et al., 2014; Huang et al., 2014). Parameters that are being analyzed in such sensors include fluorescence intensity, decay time, quenching efficiency and regeneration of fluorescence or luminescence energy transfer. Among these, the most innovative and recently evolved optical biosensors are those based on surface plasmon resonance (SPR) properties using different gold nanocomposites (Kawaguchi et al., 2008; Lee et al., 2015; Singh and Strouse, 2010; Yeom et al., 2013). These biosensors have been widely used in the fields for detection of infectious diseases related with cells, bacteria or viruses (Ahmed et al., 2016; Guo et al., 2015; Lee et al. 2018; Oh et al., 2017). Generally, fluorescent quantum dots (QDs) have been widely applied as fluorescence reporters in various LSPR based biosensor whereas the SPR generated AuNPs plays the crucial role to influence the fluorescence signal depending on the size, shape and distance (Lee et al., 2015; Takemura et al., 2017). Triggering with the analyte, it can alter the position as well as distance between these two nanocomponents (QDs and AuNPs), resulting in the variation of signal detection.

There are many attempts on optical sensing which are reported on virus detection (Chang 2010 et al., 2010; Lee et al., 2015; Takemura et al., 2017) as the conventional diagnostic systems still have certain limitations. Induced antibody detection on serological analysis can lead to false negative or false positive misguided data interpretation (Tate et al., 2004). Most authentic viral culture analysis is time consuming whereas immunofluorescence assays are limited to their sensitivity. Therefore, there is an utmost need for the development of rapid, highly sensitive and selective diagnostic sensor for the virus detection. Pang et al., (2015) reported a fluorescent aptasensor system for the sensitive detection of influenza virus H5N1 in human serum by guanine-enriched anti-rHA aptamers immobilized on the surface of the $Ag@SiO_2$ nanoparticles which performed as a metal-enhanced fluorescence sensing platform. Similarly, Wu et al., (2015) developed an enzyme-induced bi-functional magnetic electrochemical immunosensor to detect Influenza virus A (H7N9) in complex media. In our previous work, detection of influenza virus A (H1N1) has been reported on a combination of LSPR-induced optical transduction from antibody-labeled AuNPs and the fluorescence signal generated from adjacent antibody-conjugated CdSeTeS QDs (Takemura et al., 2017). However, using several antibodies or aptamer-conjugated antibodies is making those systems complicated and expensive. Moreover, the high fluorescence signal of background also hampers the enhancement of surface plasmon signal, which is disadvantage of this method. To overcome this, here we have developed a new method of LSPR-induced optical transduction between AuNPs and CdSeTeS QDs with a single step process to detect NoV-LPs and Norovirus (NoV). The covalent attachment between AuNPs and CdSeTeS QDs forms the rigid sensing probe of CdSeTeS QDs/AuNPs which can sufficiently decreases the nonspecific interaction, resulting the increasing sensitivity. NoV which is mostly common causes for gastroenteritis disease, generally transmitted through shellfish consumption and food and waterborne routes (Bitler et al., 2013). As the levels of enteric viruses in bivalve

mollusk or in mussels are generally in very low concentration, the high sensitive technique is in demand for its early detection. To establish the detection technique, initially we have taken the NoV-LPs as a target analyte, because there is no robust cell culture system for the NoV propagation to date. The anti-Nov antibody-conjugated CdSeTeS QDs are covalently linked with AuNPs, quenching the fluorescence of CdSeTeS QDs/AuNPs nanocomposites which has been used as the sensing probe for a single step label free detection of NoV-LPs and NoV. The detection mechanism of the biosensor involves the regeneration of quenched fluorescence of CdSeTeS QDs/AuNPs due to LSPR while the attached NoV creates steric hindrance between two nanomaterials as depicted in Scheme 1.

2. Methods and Materials

2.1. Materials

PBS buffer, sodium citrate, polyoxyethyelene (20), sorbitan monolaurate (Tween 20), hydrogen peroxide, sulfuric acid, methanol, potassium hydroxide (KOH), tri-sodium citrate, chloroform and acetone were purchased from Wako Pure Chemical Ind. Ltd. (Osaka, Japan). Tetramethylbenzidine (TMBZ) was purchased from Dojindo (Kumamoto, Japan). $HAuCl_4$, *N*-(3-dimethylaminopropyl)-*N*-ethylcarbodiimide hydrochloride (EDC), *N*-hydroxysuccinimide (NHS), bovine serum albumin (BSA), 11-mercaptoundecanoic acid (MUDA), 1-octadecene, cadmium oxide (CdO), tellurium (Te), L-cysteine, hexadecylamine (HDA), trioctylphosphine oxide (TOPO), trioctylphosphine (TOP), selenium (Se) and sulfur (S) were purchased from Sigma Aldrich Co., LLC (Saint Louis, MO, USA). Oleic acid was purchased from Nacalai Tesque Inc. (Kyoto, Japan). Goat anti-rabbit IgG-horseradish peroxidase (HRP) was purchased from Santa Cruz Biotechnology (CA, USA). Anti-NoV antibody broadly reactive to GII.4 (NS14 Ab) (Kitamoto et al. 2002; Kou et al. 2015) was

used for this work. Zikavirus and influenza virus A (H3N2) for selectivity test were kindly provided by Professor K. Morita of Institute of Tropical Medicine Nagasaki University and Dr. C. Kawakami of the Yokohama City Institute of Health (Yokohama Japan), respectively.

2.2. Synthesis of CdSeTeS QDs

Organometallic hot-injection synthesis of quaternary-alloyed CdSeTeS QDs was carried out according to our previously reported method using CdO, Se, S as the basic precursors (Adegoke et al., 2015).

2.3. Capping of CdSeTeS QDs

To make the hydrophilic QDs from the synthesized hydrophobic CdSeTeS QDs and to functionalize its surface with amine group, the L-cysteine was conjugated via a ligand exchange reaction. A methanolic-KOH-L-cysteine solution was prepared by dissolving 3 g of KOH in 40 mL of methanol and 2 g of L-cysteine. The hydrophobic QDs in chloroform solution were added to the methanolic-KOH-L-cysteine solution, and an appropriate volume of ultrapure deionized (DI) water was added to precipitate the hydrophilic QDs from solution. The solution was stirred for several mins and was allowed to stand overnight for complete separation of the organic phase from the water-soluble phase. The QDs were repeatedly purified using acetone and chloroform.

2.4. Synthesis of AuNPs

For the preparation of AuNPs, 35 µL of 2 mM $HAuCl_4$ and finally 300 µL of 100 mM tri-sodium citrate were added into 25 mL of pure boiling water under vigorous stirring condition (Zhao et al., 2008). The whole solution was boiled and stirred for 15 min until the color changes to pink.

2.5. Functionalization of AuNPs with 11-mercaptoundecanoic acid

The AuNPs was attached with the MUDA to generate carboxylic acid group in to the surface. The AuNPs solution was stirred for 2 h with 0.1 mM of MUDA at pH 3 where the thiol group has been covalently linked with the AuNPs via soft acid soft base interaction. After successful synthesis of the AuNP-MUDA, the nanoparticle was washed several times with DI water and centrifuged at 6000 × g to obtain excess MUDA free AuNPs.

2.6. Synthesis of sensing probe

Initially, the anti-NoV antibody was conjugated with the free carboxylic group of L-cysteine capped CdSeTeS QDs via EDC/NHS covalent chemistry. Then, the MUDA functionalized AuNPs was covalently linked with the free amine group of L-cysteine capped antibody-linked QDs via EDC/NHS reaction (Valeur and Bradley, 2009). In brief, EDC was mixed with the carboxylic functionalized AuNPs and then further activated with NHS for 30 min before addition of the antibody conjugating QDs (Ab-QDs). The conjugate mixture was stirred overnight at 7°C to form antibody-conjugating nanocomposites (Ab-CdSeTeS QD/AuNPs) which were purified by centrifugation (3000 × g) for 5 min and subsequently dissolved in 2 mL of ultrapure DI water.

2.7. Enzyme linked immunosorbent assay (ELISA)

Antibody conjugation on the CdSeTeS QD/AuNPs nanocomposite was confirmed by conventional ELISA test in a nonsterile polystyrene 96-well flat-bottom microtiter plate (Becton Dickinson Labware, NJ, USA). The Ab-CdSeTeS QD/AuNPs nanocomposite was tested before and after NoV-LP addition along with its negative controls of bare QDs, AuNPs, BSA and DI water. After coating of each component in the well bottom, 100 µL of 5 % skim milk solution was added as a blocking agent to each well after washing 3 times with PBS buffer, containing 0.1 % Tween 20. After blocking, the skim milk was removed by washing 3 times with the buffer. Then, anti-rabbit IgG-HRP was diluted to 1:4000 with 2 % BSA, and

100 µL of this solution were added was and incubated for 1 h. This secondary antibody was used to bind with the primary anti-NoV antibody which was conjugated on the surface of QDs as the purpose of this ELISA was to determine the conjugation of the primary antibody. 3,3',5,5'-tetramethylbenzidine or TMB (100 µL) was then added to the each well which was initiated by its characteristic blue coloration. The reaction was then stopped by adding 50 µL of 10 % H_2SO_4, which changed the color of the solution from blue to yellow due to its diimine formation. The absorbance of the solution was measured using a microplate reader at 450 nm with a reference filter of 655 nm.

In later part, to compare the detection ability of our proposed sensor, three spiked samples of clinically isolated NoVs along with two different concentrations of NoV-LPs were tested by commercial ELISA kit (Denka Seiken Co Ltd., Model No. 324603, Niigata, Japan).

2.8. Physicochemical analysis

To check the size and surface morphology, transmission electron microscopy (TEM) images were obtained using a TEM (JEM-2100F; JEOL, Ltd., Tokyo, Japan) operated at 100 kV. UV-Vis absorption and fluorescence emission measurements were carried out using a filter-based multimode microplate reader (Infinite® F500; TECAN, Ltd, Männedorf, Switzerland). Powder X-ray diffraction (PXRD) analysis was carried out using a RINT ULTIMA XRD (Rigaku Co., Tokyo, Japan) with a Ni filter and a Cu-Kα source. Dynamic light scattering (DLS) measurements were performed using a Zetasizer Nano series (Malvern Inst. Ltd., Malvern, UK). Conjugation of the antibody to the Ab-QDs and Ab-CdSeTeS QD/AuNPs nanocomposites were confirmed using a plate reader from Bio-Rad (Model 680; Hercules, USA).

2.9. Preparation of NoV-LPs and clinically isolated NoVs

NoV-LPs were prepared according to the standard method of VLP preparation (Ahmed et al., 2016; Jiang et al., 1992). Clinically isolated NoVs were collected from fecal samples of the patients with infectious gastroenteritis, including foodborne illness, by inspections based on laws and ordinances. This NoV sampling was carried out according to the guideline, after getting the approval by Ethics Committee of Environment and Hygiene Institute in Shizuoka Prefecture (September 14, 2016).

2.10. Fluorometric sensing of NoV-LPs and clinically isolated NoVs using the CdSeTeS QD/AuNPs sensing probe

CdSeTeS QD/AuNPs nanocomposite was mixed in different concentration of 20 µL volume of the target NoV-LPs as well as clinically isolated NoVs and incubated for 1 min before fluorescence measurements were acquired. The detection of NoV-LPs in the concentration range of 1×10^{-14} – 1×10^{-7} g mL^{-1} was carried out in DI water. The sample solution was excited at 450 nm, and the fluorescence intensity was measured in a range of 500 – 700 nm. The human serum was diluted 10 times before to spike the NoV-LPs in to it. Clinically isolated NoVs were also detected with the sensor probe in the similar way to measure the fluorometric response.

2.11. Quantification of clinically isolated NoVs using real-time PCR

NoV RNAs were extracted from 10 % fecal suspension in PBS by using QIAamp Viral RNA Mini Kit (QIAGEN, Tokyo Japan), and after treated with recombinant DNase (RNase-free) (TaKaRa Bio Inc., Shiga, Japan), reverse transcription was performed by using Prime Script RT Reagent Kit (Perfect Real Time) (TaKaRa Bio Inc.). Obtained cDNAs were detected and quantified by real-time PCR technique by using Premix EX Taq (Probe qPCR) (TaKaRa Bio Inc.) in accordance with the notice of the Ministry of Health, Labor and Welfare, Japan (2003).

3. Results and discussion

The central theme in this work is to build a new and simple method to detect virus directly without any pretreatment of analytes. Here, we have successfully synthesized an Ab-CdSeTeS QD/AuNPs sensing probe which is able to detect the NoV-LPs by measuring the fluorescence intensity after 1 min of the sensor probe addition (as depicted in Scheme 1). Due to the covalent attachment between CdSeTeS QDs and AuNPs, it causes strong fluorescence quenching of the QDs, initially. After addition of different virus concentration, the Ab-CdSeTeS QD/AuNPs bind with the target due to the presence of monoclonal antibody in between the QDs and AuNPs. This antibody-antigen interaction induces steric hindrance, which causes the optimum distance for LSPR between these two nanoparticles, resulting fluorescence enhancement. The enhancement is proportionated with the concentration of the target NoV-LPs as well as in real NoV analytes, confirming proficient detection ability of the proposed nanobiosensor. Unlike other conventional methods of LSPR detection, here, the sensor nanocomposite is conjugated with a single antibody and capable to detect the virus, without any pre-treatment just after addition in to the sensing sample.

3.1. Synthesis of sensing probe and characterizations

The morphology as well as size distribution of two individually synthesized nanoparticles was examined first. The shape and morphological properties of the CdSeTeS QDs were analyzed using TEM. A monodisperse particle distribution is observed while the particle shape is consistently spherical across the entire TEM image (Fig. 1A). The particle size distribution has been given in the inset of Fig. 1A where the highly homogenous distribution is found in the range of 3 – 9 nm with the average particle size of 5.9 ± 0.6 nm. The UV-Vis spectrum of the synthesized CdSeTeS QDs is given in the supplementary

information (Fig. S1), showing the signature absorption hump of CdSeTeS QDs even after the antibody conjugation which confirms the successful synthesis. Similarly, the citrate stabilized AuNPs are also evenly distributed in the range of 7 – 15 nm with the average particle size of 11.4 ± 0.5 nm (Fig. 1B). A single TEM image of an isolated AuNP is given in the inset of Fig. 1B where it is clearly seen the exact spherical nature of the AuNPs. After incorporation with the MUDA, the agglomeration has been reduced to some extent due to the coating of the organic layer on the surface. The capping of the organic layer is verified by the UV-Vis spectra, presented in the Fig. S2. After successful preparation of the Ab-CdSeTeS QD/AuNPs with anti-Nov antibody conjugation, the nanocomposite was further characterized by TEM. In Fig. 1C, it is clearly observed that the small sized QDs (~5 nm) and AuNP (~12 nm) are closely situated due to the covalent attachment controlled by the short linker of MUDA. As the concentration of the AuNPs is comparatively less than the QDs concentration, the relatively high amounts of QDs are found near the CdSeTeS QD/AuNPs cluster. The anti-NoV antibody conjugation with the CdSeTeS QD/AuNPs nanocomposites was confirmed by ELISA (Fig. 1D). The absorbance peak in ELISA of the bare CdSeTeS QDs is negligible as expected. The antibody loading is increased to the highest level in case of Ab-CdSeTeS QD/AuNP, confirming the successful antibody conjugation. However, after the NoV-LPs loading, the ELISA signal is decreased obviously due to the less availability of the active site of the NoV-LPs covered Ab-CdSeTeS QD/AuNPs nanocomposites. Overall, the ELISA of different stages of CdSeTeS QD/AuNPs supports the successful conjugation of antibodies with the nanocomposites.

The CdSeTeS QD/AuNPs nanocomposites were further characterized by XRD spectra to illustrate the crystal nature of the QD nanocrystals. The diffraction pattern of the QDs indicates that the QDs are crystalline and cubic in nature (Fig. 2A), exhibiting three characteristic peaks at 2theta of 24.9°, 42.3° and 50.6° for (111), (220) and (311) crystal

planes respectively (Adegoke et al., 2015; Li et al., 2016; Yang et al., 2013). The position of all these peaks remains unchanged after functionalization with AuNPs, indicating that the attachment only takes place in the functional groups of the CdSeTeS QD nanocomposites without affecting the crystal structure. In addition, a small but clear peak at 2theta = 37.9° has been introduced due to the incorporation of the (111) plane of AuNPs on the nanocomposites (Krishnamurthy et al., 2014), supporting the successful formation of the CdSeTeS QD/AuNPs nanocomposites.

The hydrodynamic diameter as well as the dispersity of CdSeTeS QD/AuNPs nanocomposites along with its individual components was determined by DLS (Fig. 2B). The distribution of the AuNPs and MUDA-AuNPs are shown particle size of 8.5 ± 1.1 nm and 11.2 ± 1.2 nm, respectively. It proves the monodisperse nature of AuNPs which is not altered even after conjugation with MUDA. Similarly, the cysteine capped CdSeTeS QDs and antibody-conjugated QDs show the hydrodynamic diameter of 29.4 ± 2.3 and 54.2 ± 3.4 nm respectively which differs from the size distribution finding in TEM images. This may be due to the fact that being a small sized and charged particles, the QDs have a strong tendency to agglomerate in aqueous medium, increasing the hydrodynamic radius (Reghuram et al., 2015). However, after the conjugation of these two nanoparticles, the Ab-CdSeTeS QD/AuNPs nanocomposite shows the diameter of 102.1 ± 3.2 nm which is increased up to 107 ± 2.2 nm after the NoV-LPs attachment, confirming the agglomerated distribution, further supported by TEM image, later.

3.2. Optimization of CdSeTeS QD/AuNPs sensor and its mechanism of sensing

After proper characterizations, the Ab-CdSeTeS QD/AuNPs nanocomposite has been used as the fluorometric sensor probe for NoV-LPs detection. Being a strong inorganic QDs with high quantum yield of 0.57 (Takemura et al., 2017), the bare Ab-CdSeTeS QDs show a

strong fluorescence signal at 640 nm at the excitation of 450 nm (Fig. 2C). After the covalent attachment with AuNPs, the spectral intensity of Ab-CdSeTeS QDs has been quenched more than 65 % due to the close interaction with AuNPs. The spectral overlap between the surface plasmon spectrum of AuNPs and the emission spectrum of CdSeTeS QDs confirms the quenching interaction, given in Fig. S3. However, after successive addition of NoV-LPs on the nanocomposites, a significant enhancement of the fluorescence signal has been observed due to the enhanced distance between AuNPs and QDs which is the key mechanism of virus detection. It is well known fact that the LSPR properties between any two nanoparticles are highly dependent on their distance and sizes (Guo et al., 2015). Here, the size of QDs and AuNPs are always kept constant at ~6 nm and 12 nm respectively. Therefore, the distance between these two nanoparticles plays the major role of altering fluorescence intensity of QDs. Due to the covalent attachment through a small organic chain of MUDA, the AuNPs and the CdSeTeS QDs are situated in a very closely packed structure (within 6 nm distance), resulting in the strong fluorescence quenching of the QDs. However, after the NoV-LPs addition, the NoV-LPs are bound to the Ab-CdSeTeS QD/AuNP due to the antibody-NoV-LPs conjugation. The binding of the large size of NoV-LPs in between the AuNPs and QDs, induces strong steric repulsion. Therefore, the closely packed structure cannot be retained which creates larger distance between these two nanoparticles, initiating the LSPR mediated fluorescence enhancement.

In most cases of virus detection methods on LSPR, the nanomaterials are conjugated with different specific bio-markers or antibodies, corresponding to the analyte. After analyte addition, the nanomaterials get close towards each other using analyte as a bridge molecule. In this case, QDs are existed and shows high fluorescence intensity before inducing LSPR in the detection system, which is background fluorescence intensity of detection system. In spite of using more than one costly biomarkers or antibodies in which the antibody/aptamer linked

analyte bridged system highly suffers from non-specific interaction between two nanomaterials, resulting high background signal hence lowering sensitivity. However, here we have made the system rigid by covalent bonding between two nanomaterials initially, which causes strong fluorescence quenching of the QDs. Then, the steric repulsion induced by large sized analyte virus particles introduces the required distance replacement which feeble the quenching behavior, resulting LSPR induced fluorescence enhancement recovers fluorescence.

To optimize the exact size for best results, we have varied the sizes of interacting AuNPs from 5 to 100 nm, maintaining the constant size of CdSeTeS QDs for the detection of 1×10^{-9} g mL^{-1} NoV-LPs. LSPR effect is highly depended on many factors like the properties of QDs, size and shape of AuNPs, concentration of AuNPs and QDs, ratio etc. (Li et al., 2011; Singh et al., 2010). Therefore, as shown in Fig. 2D, quenching effect was found almost similar for all different sizes of AuNPs (5, 12, 20, 40, 80, 100 nm) while the 12 nm sized AuNPs shows best quenching afterward enhancement effects on CdSeTeS QDs. In the case of bigger AuNPs, the surface resonance orbital overlap is too big compared to small sized AuNPs. Therefore, small perturbation, triggered by the attached NoV-LPs could not able to move the sufficient distance, required for fluorescence enhancement. Therefore, evaluating the enhancement as well as quenching factor, the 10 – 12 nm AuNPs has been chosen to get best performance for this work.

3.3. Fluorometric sensing of NoV-LPs using the Ab-CdSeTeS QD/AuNPs sensing probe

Detection of the NoV-LPs was carried out to demonstrate the performance of the sensor probe. The LSPR-induced immunofluorescence enhancement for the detection of NoV-LPs and its calibration curve is given in Figs. 3A and B, respectively. The fluorescence at 640 nm of CdSeTeS QDs has been monitored as sensing signal whose intensity is quenched and

thereafter enhanced by adjacent AuNPs. At increasing concentrations of NoV-LPs, progressive enhancement of the fluorescence has been achieved without any notable peak shift, providing evidence that the QDs were highly stable during the detection period. The response time is around 1 min after the addition of the target NoV-LPs. The corresponding linear calibration curve is shown in Fig. 3B where the limit of detection (LOD) is found of 12.1×10^{-15} g mL^{-1}, based on $7\sigma L$ (σ is the standard deviation of the lowest signal and L is the lowest concentration used).

To verify the LSPR behavior from AuNPs influences, the sensitivity of the biosensor was further carried out by a control test using Ab-CdSeTeS QD. Instead of covalently bonded AuNPs, the AuNPs was only physically mixed with the Ab-CdSeTeS QDs for the detection of the targeted NoV-LPs. As shown in Fig. S4, the fluorescence emission of the Ab-CdSeTeS QDs after addition of AuNPs by only physical mixing was almost unaffected, indicating that without LSPR signal, the target virus cannot be detectable. The changes of fluorescence intensity of the Ab-CdSeTeS QD/AuNPs have been also observed in naked eye in the 450 nm UV light chamber (Fig. 3C). The highly flourished bare Ab-CdSeTeS QDs is significantly quenched after the formation of CdSeTeS QD/AuNPs nanocomposites. However, after addition of 1×10^{-9} g mL^{-1} NoV-LPs, the enhancement of fluorescence is also observed which confirms the LSPR induced phenomenon. The TEM images of Ab-CdSeTeS QD/AuNPs/NoV-LPs are given in Fig. 3D where the agglomerated Ab-CdSeTeS QD/AuNPs nanocomposites are situated clearly on ~40 nm NoV-LPs surface. For comparison, the TEM image of only NoV-LPs has provided in Fig. S5 of supporting information. The higher magnification of the CdSeTeS QD/AuNPs/NoV-LPs image of an isolated particle (inset of Fig. 3D) clearly demonstrates the formation of the NoV-LPs conjugated nanocomposites which support our hypothesis.

From the aspect of the wide detection range, low LOD and short response time, our nanobiosensor shows much better performances compared with recently published reports on LSPR based sensors as well as other methods, listed in Table 1. In our previous study of LSPR detection, interaction of the target virus with Ab-conjugated AuNPs and other Ab-conjugated QDs induces an LSPR signal from adjacent AuNPs to trigger fluorescence-enhancement changes in the QDs in proportion to the concentration of the target virus. Though the excellent linearity has been achieved in that case, however due to the existence of free QDs in detection solution, the background signal was quite high, resulting higher LOD of 30×10^{-15} g mL^{-1}. In this present study, the system was made rigid by covalent bonding between two nanomaterials which initially exhibited strong fluorescence quenching of QDs. Due to the rigid structure of our Ab-CdSeTeS/AuNPs nanocomposite, the possibility of nonspecific interaction is very low and the sensor cannot generate any enhancement until the analytes are added, resulting very low background signal, hence high sensitivity. Therefore, the system is able to show fluorescence enhancement even after addition of very small number of virus particles, ensuing low detection limit of 12.1×10^{-15} g mL^{-1}. In addition, the rapid detection with high sensitivity of this proposed sensor displays clear advantages over the conventional methods of enzyme immunoassays, which requires ~15 – 20 min, and RT-PCR, which requires several hours for detection.

3.4. Selectivity test of the sensor

Selectivity is one of the most important parameters for real sensing application. The selectivity of the nanobiosensor for the detection of the target NoV-LPs was compared with Influenza virus A (H3N2) and Zika viruses. Two percent BSA solution, human serum and 10-fold diluted human serum samples were treated as negative control to judge the matrix effect of the biosensor (Fig. 3E). In case of most of the interferences, the matrix effects are negligible. Due to the presence of huge inferring agents, only 100% human serum affects the

fluorescence of CdSeTeS QDs a little. The matrix effect is relatively high in this case (14% compared to 1×10^{-14} g mL^{-1} of NoV-LP) which can be considered well compared with recent literatures as well as available kits. However, to get accurate interfering results, further investigations in serum samples have been carried out in 10 % diluted serum samples. Due to the structural similarities, the sensor has shown about 32 % signal enhancement for influenza virus. However, the nanobiosensor for the targeted NoV-LPs is greater than that of other viruses, demonstrating the sufficient specificity of our biosensor for the target virus. In addition, some amino acids (2 mM mL^{-1}) and metal ions (1×10^{-4} g mL^{-1}) which are common interferences for the real or clinical sample analysis are also investigated in higher concentrations and found ignorable signal for the detection analysis.

3.5. Sensing in serum sample

Human serum of 10 % was used as a detection medium to demonstrate the ability of the biosensor in a complex biological medium. The biosensor shows a similar trend of detection in the range of the spiked concentration of NoV-LPs which confirms the applicability of the sensor for the real sample monitoring (Fig. 4A). The calibration curve found from the NoV-LPs detection is plotted in Fig. 4B where the slope of linearity is little flattered with respect to the detection found in DI water samples, presented in Fig. 3B. Though the small interference of the serum matrix has lowered the slope of the calibration, decreasing of LOD value to 15.6×10^{-15} g mL^{-1} however the sensitivity is quite appreciable with respect to other reports for its real application.

3.6. Detection of clinically isolated NoV

The spiked amount of NoV from clinical sample was also detected by the CdSeTeS QD/AuNPs nanocomposites. The fluorescence intensity was gradually changed as a function of the NoV concentration, following the similar trend as NoV-LPs (Fig. 4C). A linear

calibration curve was obtained in the range $10^2 – 10^4$ copies mL^{-1} (Fig. 4D) and the detection limit was 95.0 copies mL^{-1}. This implies that the NoV from clinical sample was successfully detected by this proposed technique without compromising the efficiency. However, in case of higher NoV concentration of 10^6 copies mL^{-1}, the enhancement turns to quenching of QDs fluorescence (data not shown). This may be due to the fact that in presence of excess virus particles, some viruses themselves can entrap on the QDs surface, resulting quenching. This limits the detection range up to 10^5 copies mL^{-1}, however which is enough for its practical application. The TEM images of Ab-CdSeTeS QD/AuNPs nanocomposites with this clinically isolated NoVs are given in Fig. 4E where the successful conjugation are clearly visible with ~40–80 nm NoVs. The higher magnification image of an isolated Ab-CdSeTeS QD/AuNPs/NoV nanocomposites (inset of Fig. 4E) confirms the formation more clearly which can support our hypothesis stated earlier.

To further confirm the applicability, three spiked samples of clinically isolated NoV along with two different concentrations of NoV-LPs are tested by commercial ELISA kit and compared with the results obtained from our proposed biosensor. It is clearly shown in Fig. 4F that the commercial NoV detection kit is unable to detect the NoV concentration in lower range though it is useful for higher concentration range of $10^4 – 10^6$ copies mL^{-1}. In contrast, our proposed sensor shows excellent detectability in the low NoV concentration of $10^2 – 10^5$ copies mL^{-1}.

4. Conclusion

In this study, we have successfully synthesized a new class of nanocomposites which can detect NoV in a single-step and rapid fluorescence-based technique. In Ab-CdSeTeS QDs/AuNPs nanobiosensor, the adjacent AuNPs initially quench the fluorescence signal of the CdSeTeS QDs whereas after successful attachment of target NoV-LPs or NoV via

antibody-antigen interaction, it triggers the fluorescence enhancement of QDs. The steric repulsion induced by the analyte causes the required distance replacement for the LSPR interaction which is the key reason for obtaining higher sensitivity over other conventional LSPR based biosensors. The enhancement is proportionated with the concentration of the target NoV-LPs, maintaining a linear relationship from 10^{-14} to 10^{-9} g mL^{-1} with a LOD of 12.1×10^{-15} g mL^{-1} in DI water and 15.6×10^{-15} g mL^{-1} in human serum, confirming proficient detection of the NoV-LPs. The clinically isolated NoV from NoV-infected patients was also investigated, and the corresponding sensitivity was found 95.0 copies mL^{-1}. The easily applicable method of this proposed biosensor can be applied not only for the detection of NoV but also can be served as a general platform by changing the entrapped biomolecules, in the wide variety of other sensing application in future.

Acknowledgement

Authors thank Professor K. Morita of Institute of Tropical Medicine Nagasaki University and Dr. C. Kawakami of the Yokohama City Institute of Health (Yokohama Japan) for kindly providing Zika virus and influenza virus A (H3N2) for selectivity test, respectively. ADC (No. P17359), JL (No. P16361) and OA (No. 26-04354) thank the Japan Society for the Promotion of Science (JSPS) for a postdoctoral fellowship. This work was supported and partly by the Bilateral Joint Research Project of the JSPS, Japan.

Appendix A: Supplementary data

References

Adegoke, O., Nyokong, T., Forbes, P.B., 2015. Structural and optical properties of alloyed quaternary CdSeTeS core and CdSeTeS/ZnS core–shell quantum dots. J. Alloys Compd. 645, 443–449.

Ahmed, S.R., Kim, J., Suzuki, T., Lee, J., Park, E.Y., 2016. Enhanced catalytic activity of gold nanoparticle-carbon nanotube hybrids for influenza virus detection Biosens. Bioelectron. 85, 503–508.

Al-Ogaidi, I., Gou, H., Aguilar, Z. P., Guo, S., Melconian, A. K., Al-Kazaz, A. K. A., Meng, F., Wu, N., 2014. Detection of the ovarian cancer biomarker CA-125 using chemiluminescence resonance energy transfer to graphene quantum dots Chem. Commun. 50, 1344–1346.

Anh, N. T. N., Chowdhury, A. D., Doong, R. A., 2017 Highly sensitive and selective detection of mercury ions using N, S-codoped graphene quantum dots and its paper strip based sensing application in wastewater. Sens. Actuators, B 252, 1169–1178.

Batule, B. S., Kim, S. U., Mun, H. M., Choi, C., Shim, W., Kim, M., 2018. Colorimetric detection of norovirus in oyster samples through DNAzyme as a signaling probe, J. Agric. Food Chem., 66, 3003–3008.

Bitler, E. J., Matthews, J. E., Dickey, B. W., Eisenberg, J. N. S., Leon, J. S., 2014. Norovirus outbreaks: a systematic review of commonly implicated transmission routes and vehicles., Epidemiol Infect., 141, 1563–1571.

Chand, R., Neethirajan, S., 2017. Microfluidic platform integrated with graphene-gold nano-composite aptasensor for one-step detection of norovirus, Biosens. Bioelectron. 98, 47–53.

Chang, Y. F., Wang, S. F., Huang, J. C., Su, L. C., Yao, L., Li, Y. C., Wu, S. C., Chen, Y. M.A., Hsieh, J. P., Chou, C., 2010. Detection of swine-origin influenza A (H1N1) viruses using a localized surface plasmon coupled fluorescence fiber-optic biosensor Biosens. Bioelectron. 26, 1068–1073.

Chowdhury, A. D., De, A., Chaudhuri, C. R., Bandyopadhyay, K., Sen, P., 2012. Label free polyaniline based impedimetric biosensor for detection of E. coli O157: H7 Bacteria Sens. Actuators, B 171, 916–923.

459 Dutta Chowdhury, A., Agnihotri, N., Doong, R. A., De, A., 2017. Label-free and
460 nondestructive separation technique for isolation of targeted DNA from DNA–protein
461 mixture using magnetic Au–Fe_3O_4 nanoprobes Anal. Chem. 89, 12244–12251.
462 Dutta Chowdhury, A., Doong, R. A., 2016. Highly sensitive and selective detection of
463 nanomolar ferric ions using dopamine functionalized graphene quantum dots ACS Appl.
464 Mater. Inter. 8, 21002–21010.
465 Ganganboina, A. B., Dutta Chowdhury, A., Doong, R. A., 2018. N-doped graphene quantum
466 dots decorated V_2O_5 nanosheet for fluorescence turn off-on detection of cysteine ACS
467 Appl. Mater. Inter. 10, 614–624
468 Guo, L., Jackman, J. A., Yang, H. H., Chen, P., Cho, N. J., Kim, D. H., 2015. Strategies for
469 enhancing the sensitivity of plasmonic nanosensors Nano Today 10, 213–239.
470 Han, K. N., Choi, J. S., Kwon, J., 2016. Three-dimensional paper-based slip device for one-
471 step point-of-care testing Sci. Rep. 6, 25710.
472 Han, Z., Chen, L., Weng, Q., Zhou, Y., Wang, L., Li, C., Chen, J., 2018. Silica-coated gold
473 nanorod@CdSeTe ternary quantum dots core/shell structure for fluorescence detection
474 and dual-modal imaging. Sens. Actuators, B 258, 508–516.
475 Hsu, C. L., Lien, C. W., Wang, C. W., Harroun, S. G., Huang, C. C., Chang, H. T., 2016.
476 Immobilization of aptamer-modified gold nanoparticles on BiOCl nanosheets: tunable
477 peroxidase-like activity by protein recognition Biosens. Bioelectron. 75, 181–187.
478 Huang, Y., Hu, F., Zhao, R., Zhang, G., Yang, H., Zhang, D., 2014. Tetraphenylethylene
479 conjugated with a specific peptide as a fluorescence turn-on bioprobe for the highly
480 specific detection and tracing of tumor markers in live cancer cells Chem. Eur. J. 20,
481 158–164.
482 Jiang, X., Wang, M., Graham, D.Y., Estes, M. K., 1992. Expression, self-assembly, and
483 antigenicity of the Norwalk virus capsid protein. Virol. J. 66, 6527–6532

Kawaguchi, T., Shankaran, D. R., Kim, S.J., Matsumoto, K., Toko, K., Miura, N., 2008. Surface plasmon resonance immunosensor using Au nanoparticle for detection of TNT Sens. Actuators, B 133, 467–472.

Kitamoto, N., Tanaka, T., Natori, K., Takeda, N., Nakata, S., Jiang, X., Estes, M. K., 2002. Cross-reactivity among several recombinant calicivirus virus-like particles (VLPs) with monoclonal antibodies obtained from mice immunized orally with one type of VLP. J. Clin Microbiol. 40, 2459–2465.

Kou, B., Huang, W., Neill, F. H., Palzkill, T. G., Estes, M. K., Atmar, R. L., 2015. Norovirus antigen detection with a combination of monoclonal and single chain antibodies. J. Clin Microbiol. 53, 3916–3918.

Krishnamurthy, S., Esterle, A., Sharma, N.C., Sahi, S.V., 2014. Yucca-derived synthesis of gold nanomaterial and their catalytic potential Nanoscale Res. Lett. 9, 627.

Kuila, T., Bose, S., Khanra, P., Mishra, A. K., Kim, N. H., Lee, J. H., 2011. Recent advances in graphene-based biosensors Biosens. Bioelectron. 26, 4637–4648.

Lee, J., Adegoke, O., Park, E. Y., 2018. High-performance biosensing systems based on various nanomaterials as signal transducers, Biotechnol. J. DOI: 10.1002/biot.201800249.

Lee, J., Ahmed, S. R., Oh, S., Kim, J., Suzuki, T., Parmar, K., Park, S. S., Lee, J., Park, E. Y., 2015. A plasmon-assisted fluoro-immunoassay using gold nanoparticle-decorated carbon nanotubes for monitoring the influenza virus Biosens. Bioelectron. 64, 311–317.

Lee, J. H., Huh, Y. M., Jun, Y. W., Seo, J. W., Jang, J. T., Song, H. T., Kim, S., Cho, E. J., Yoon, H. G., Suh, J. S., 2007. Artificially engineered magnetic nanoparticles for ultra-sensitive molecular imaging Nat. Med. 13, 95–99.

Li, M., Cushing, S. K., Wang, Q., Shi, X., Hornak, L.A., Hong, Z., Wu, N., 2011. Size-dependent energy transfer between CdSe/ZnS quantum dots and gold nanoparticles J. Phys. Chem. Lett. 2, 2125–2129.

509 Li, X., Lu, D., Sheng, Z., Chen, K., Guo, X., Jin, M., 2012. A fast and sensitive immunoassay
510 of avian influenza virus based on label-free quantum dot probe and lateral flow test strip.
511 Talanta. 100, 1–6.
512 Li, Z., Zhang, Q., Huang, H., Ren C., Pan Y., Wang, Q., Zhao, Q., 2016. RGDS-conjugated
513 CdSeTe/CdS quantum dots as near-infrared fluorescent probe: preparation,
514 characterization and bioapplication J. Nanopart. Res. 18, 373.
515 Linares, E. M., Pannuti, C. S., Kubota, L. T., Thalhammer, S., 2013. Immunospot assay
516 based on fluorescent nanoparticles for Dengue fever detection Biosens. Bioelectron. 41,
517 180–185.
518 Oh, S. Y, Heo, N. S., Shukla, S., Cho, H., Vilian, A. T. Z., Kim, J., Lee, S. Y., Han, Y. K.,
519 Yoo, S. M., Huh Y. S., 2017. Development of gold nanoparticle-aptamer-based LSPR
520 sensing chips for the rapid detection of Salmonella typhimurium in pork meat. Sci Rep. 7
521 10130.
522 Pang, Y., Rong, Z., Wang, J., Xiao, R., Wang, S., 2015. A fluorescent aptasensor for H5N1
523 influenza virus detection based-on the core–shell nanoparticles metal-enhanced
524 fluorescence (MEF) Biosens. Bioelectron. 66, 527–532.
525 Reghuram, S., Arivarasan, A., Kalpana, R., Jayavel, R., 2015. CdSe and CdSe/ZnS quantum
526 dots for the detection of C-reactive protein J. Exp. Nanosci. 10, 787–802.
527 Singh, M.P., Strouse, G.F., 2010. Involvement of the LSPR spectral overlap for energy
528 transfer between a dye and Au nanoparticle J. Am. Chem. Soc. 132, 9383–9391.
529 Takemura, K., Adegoke, O., Takahashi, N., Kato, T., Li, T. C., Kitamoto, N., Tanaka, T.,
530 Suzuki, T., Park, E. Y., 2017. Versatility of a localized surface plasmon resonance-based
531 gold nanoparticle-alloyed quantum dot nanobiosensor for immunofluorescence detection
532 of viruses Biosens. Bioelectron. 89, 998–1005.
533 Tate, J. and Ward G., 2004. Interferences in Immunoassay. Clin Biochem Rev. 25 105–120.

534 Valeur, E., Bradley, M., 2009. Amide bond formation: beyond the myth of coupling reagents
535 Chem. Soc. Rev. 38, 606–631.
536 Wu, J.C., Chen, C. H., Fu, J. W., Yang, H. C., 2014, Electrophoresis-enhanced detection of
537 deoxyribonucleic acids on a membrane-based lateral flow strip using avian influenza H5
538 genetic sequence as the model. Sensors 2014, 14, 4399–415.
539 Wu, Z., Zhou, C. H., Chen, J. J., Xiong, C., Chen, Z., Pang, D. W., Zhang, Z. L., 2015.
540 Bifunctional magnetic nanobeads for sensitive detection of avian influenza A (H7N9)
541 virus based on immunomagnetic separation and enzyme-induced metallization Biosens.
542 Bioelectron. 68, 586–592.
543 Yang, F., Xu, Z., Wang, J., Zan, F., Dong, C., Ren, J., 2013. Microwave‐assisted aqueous
544 synthesis of new quaternary−alloyed CdSeTeS quantum dots; and their bioapplications in
545 targeted imaging of cancer cells Luminescence 28, 392–400.
546 Yeom, S. H., Han, M. E., Kang, B. H., Kim, K. J., Yuan, H., Eum, N. S., Kang, S. W., 2013.
547 Enhancement of the sensitivity of LSPR-based CRP immunosensors by Au nanoparticle
548 antibody conjugation Sens. Actuators, B 177, 376–383.
549 Zeng, Q., Zhang, Y., Liu, X., Tu, L., Kong, X., Zhang, H., 2012. Multiple homogeneous
550 immunoassays based on a quantum dots-gold nanorods FRET nanoplatform. Chem
551 Commun. 48, 1781–1783.
552 Zhao, X., Cai, Y., Wang, T., Shi, Y., Jiang, G., 2008. Preparation of alkanethiolate-
553 functionalized core/shell Fe_3O_4/Au nanoparticles and its interaction with several typical
554 target molecules Anal. Chem. 80, 9091–9096.
555

Table 1. Comparison of the LSPR-based CdSeTeS QD/AuNPs biosensor with recently reported other detection methods in respect to limit, range of detection and response time.

Figure Captions:

Scheme 1. Schematic diagram for the preparation of CdSeTeS QD/AuNPs nanocomposites and its sensing mechanism towards NoV-LPs detection. The close covalent attachment of AuNPs with CdSeTeS QDs effectively quenched the fluorescence signal which has been recovered after NoV-LPs entrapment.

Fig. 1. TEM image of (A) CdSeTeS QDs (inset: particle size distribution where n=30), (B) AuNPs (inset: particle size distribution where n=30 and a single AuNPs), (C) CdSeTeS QDs/AuNPs nanocomposites and (D) ELISA of CdSeTeS QDs, CdSeTeS QDs/AuNPs before and after NoV-LPs addition.

Fig. 2. (A) XRD of CdSeTeS QDs and CdSeTeS QDs/AuNPs nanocomposites, (B) Hydrodynamic diameter of AuNPs, AuNPs-MUDA, CdSeTeS QDs, Ab-CdSeTeS QDs, Ab-CdSeTeS QDs/AuNPs and NoV-LPs loaded Ab-CdSeTeS QDs/AuNPs, (C) Fluorescence spectra of Ab-CdSeTeS QDs/AuNPs nanocomposites in comparison with bare CdSeTeS QDs and NoV-LPs loaded Ab-CdSeTeS QDs/AuNPs, (D) Effect of different size of AuNPs on the quenching and LSPR effect of Ab-CdSeTeS QDs/AuNPs nanocomposites.

Fig. 3. (A) Fluorescence emission spectra showing the detection of NoV-LPs in the concentration range of 1×10^{-14} – 1×10^{-7} g mL^{-1} using the LSPR-induced Ab-CdSeTeS QDs/AuNPs nanobiosensor, (B) Corresponding fluorescence calibration curve for detection of the NoV-LPs. Error bars denote standard deviation of 3 replicate measurements, (C) Fluorescence images of (i) bare CdSeTeS QDs, (ii) Ab-CdSeTeS QDs/AuNPs and (iii) 1 ×

579 10^{-9} g mL^{-1} NoV-LPs loaded Ab-CdSeTeS QDs/AuNPs nanocomposites in normal light and
580 the UV lamp of 450 nm (D) TEM image of NoV-LPs loaded Ab-CdSeTeS QDs/AuNPs
581 nanocomposites (inset: isolated NoV-LPs in higher magnification), (E) Selectivity test of the
582 Ab-CdSeTeS QDs/AuNPs nanobiosensor with 30 μg mL^{-1} of Influenza, 10^4 PFU mL^{-1} of
583 Zika viruses and other common amino acids and interfering metal ions.

584 **Fig. 4.** (A) Fluorescence emission spectra showing the detection of the NoV-LPs using Ab-
585 CdSeTeS QDs/AuNPs biosensor in 10% human serum and (B) its corresponding calibration
586 curve in presence of calibration line (black dots) found in DI water (shown in Fig. 3B). Error
587 bars denote standard deviation of 3 replicate measurements. (C) Fluorometric detection of
588 clinically isolated NoV in the concentration range of 10^2 to 10^6 copies mL^{-1} using the LSPR-
589 induced Ab-CdSeTeS QDs/AuNPs nanobiosensor, (D) Corresponding calibration curve for
590 detection of the NoV, (E) TEM image of NoV loaded Ab-CdSeTeS QDs/AuNPs
591 nanocomposites (inset: an isolated particle of Ab-CdSeTeS QDs/AuNPs/NoV), and (F)
592 Comparison of detection performance of the proposed method (red line) with commercial
593 ELISA kit (Lot No. 395121) (blue line and blue bars).

594

595 **Table 1.** Comparison of the LSPR-based CdSeTeS QD/AuNPs biosensor with recently
596 reported other detection methods in respect to limit, range of detection and response time.

Analytes	Linear range	LOD	Response time	References
LSPR based virus detection sensors				
Influenza (Fluorometric)	$1–10\times10^{-11}$ g mL^{-1}	3×10^{-10} g mL^{-1}	5 min	Takemura et al., 2017
Influenza (Colorimetric)	$1\times10^{-9}–1\times10^{-5}$ g mL^{-1}	1×10^{-9} g mL^{-1}	-	Ahmed et al., 2016
Influenza (Fluorometric)	$5–50\times10^{-9}$ g mL^{-1}	1.39×10^{-8} g mL^{-1}	15 min	Chang et al., 2010
NoV(paper based Colorimetric)	$1.58\times10^{5}–7.9\times10^{7}$ copies mL^{-1}	9.5×10^{4} copies mL^{-1}	10 min	Han et al., 2016
Dengue (Fluorometric)	$5–500\times10^{-9}$ g mL^{-1}	5.2×10^{-9} g mL^{-1}	45 min	Linares et al., 2013
Other virus detection sensors				
HBV (Fluorometric)	$>264\times10^{-9}$ g mL^{-1}	8.3×10^{-9} mL^{-1}	-	Zeng et al., 2012
Influenza (Fluorometric)	$0.27–12\times10^{-9}$ g mL^{-1}	9×10^{-7} g mL	30 min	Li et al., 2012
Influenza (Colorimetric)	$0.1–100\times10^{-9}$ g	1×10^{-8} g	-	Wu et al., 2014
NoV (Fluorometric)	2–18 copies mL^{-1}	1.2 copies mL^{-1}	3 min	Han et al., 2018
NoV (Microfluidic)	$1\times10^{-10}–3.5\times10^{-9}$ M	1×10^{-11} M	40 min	Chand et al., 2017
Nov (Colorimetric)	$10–10^{4}$ copies mL^{-1}	1 copy mL^{-1}	-	Batule et al., 2018
NoV-LPs (Fluorometric)	**$1\times10^{-14}–10^{-9}$ g mL^{-1}**	**12.1×10^{-14} g mL^{-1}**	**1 min**	**This work**
NoV (Fluorometric)	**$10^{2}–10^{5}$ copies mL^{-1}**	**95.0 copies mL^{-1}**		

597

Nasrin et al., Graphical Abst

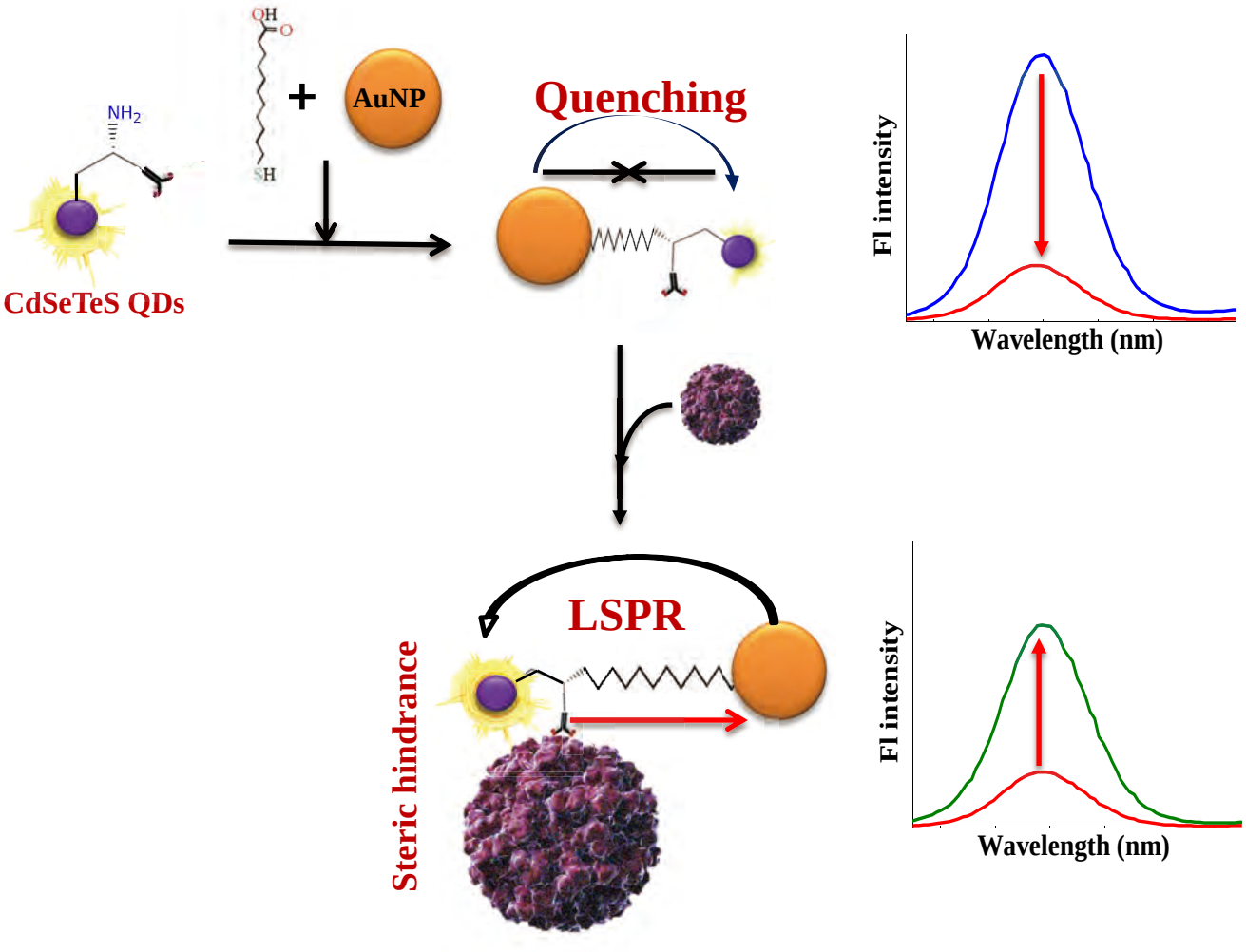

Nasrin et al., Scheme 1

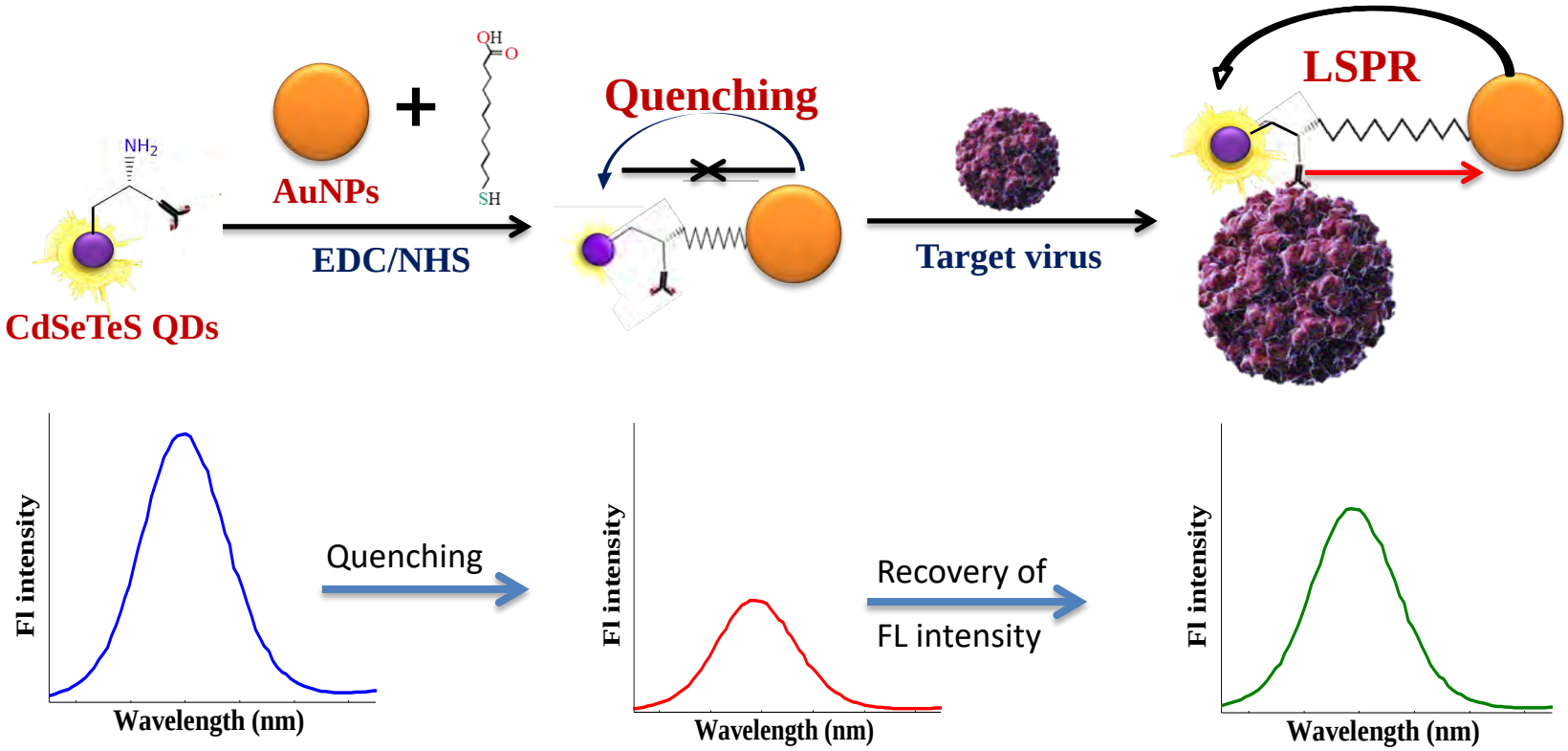

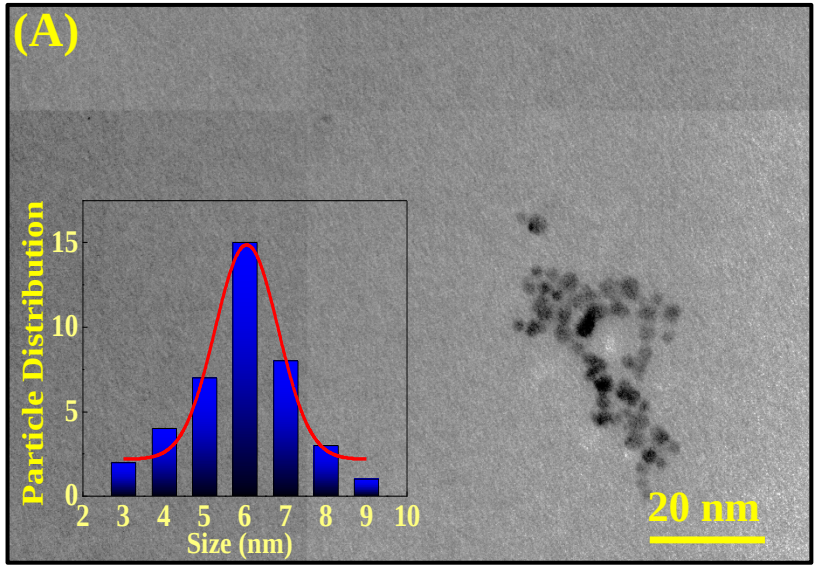
(A)
Particle Distribution
0
5
10
15
2 3 4 5 6 7 8 9 10
Size (nm)
20 nm

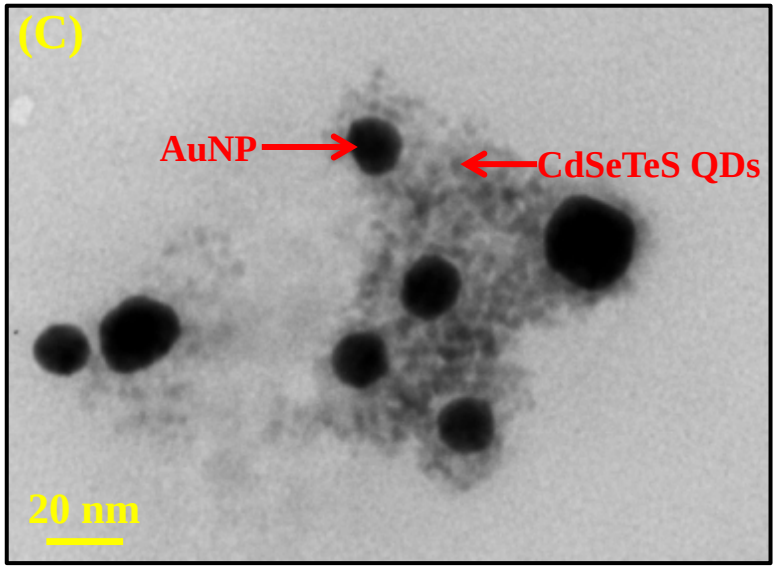
(C)
AuNP
CdSeTeS QDs
20 nm

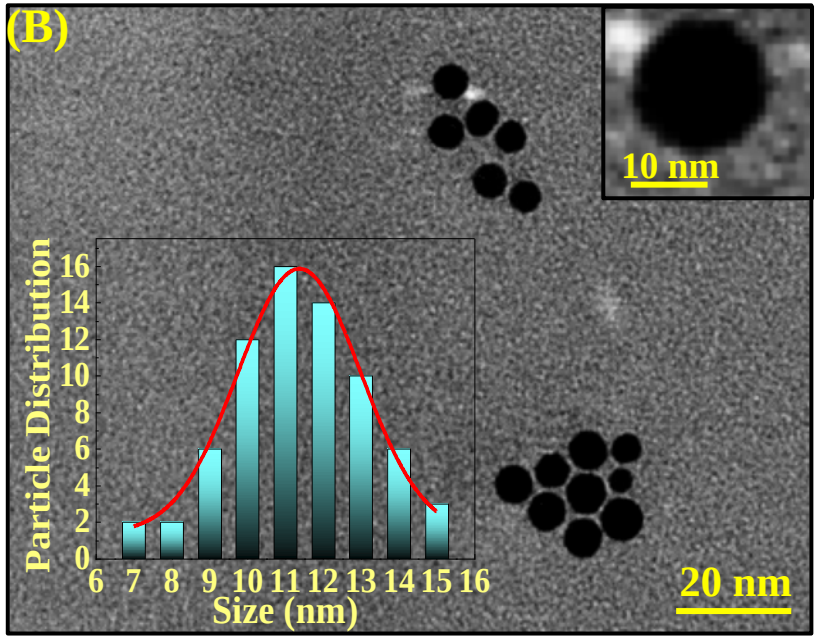
(B)
10 nm
Particle Distribution
0
2
4
6
8
10
12
14
16
6 7 8 9 10 11 12 13 14 15 16
Size (nm)
20 nm

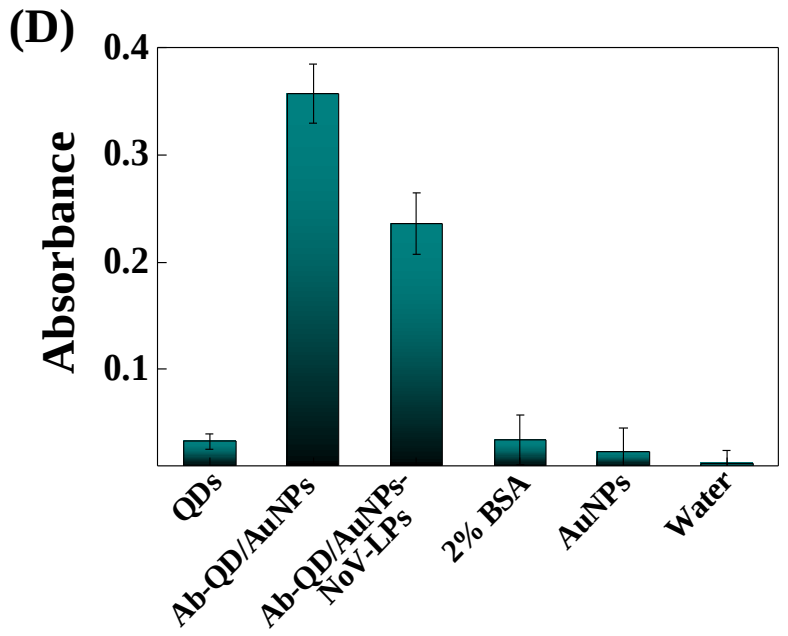
(D)
Absorbance
0.1
0.2
0.3
0.4
QDs
Ab-QD/AuNPs
Ab-QD/AuNPs-NoV-LPs
2% BSA
AuNPs
Water

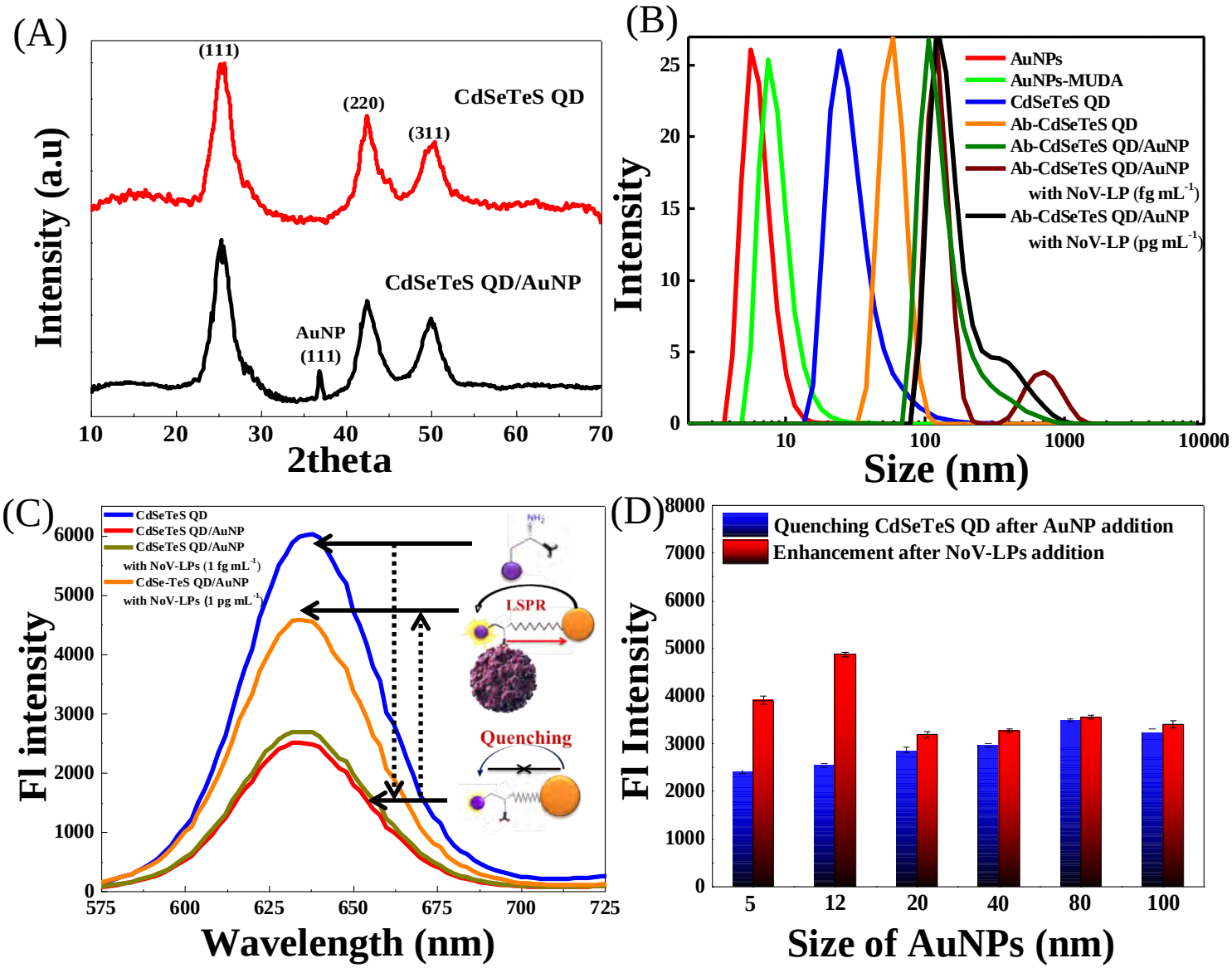
(A)
(111)
(220)
(311)
CdSeTeS QD
CdSeTeS QD/AuNP
AuNP
(111)
Intensity (a.u)
2theta
(B)
AuNPs
AuNPs-MUDA
CdSeTeS QD
Ab-CdSeTeS QD
Ab-CdSeTeS QD/AuNP
Ab-CdSeTeS QD/AuNP with NoV-LP (fg mL-1)
Ab-CdSeTeS QD/AuNP with NoV-LP (pg mL-1)
Intensity
Size (nm)
(C)
CdSeTeS QD
CdSeTeS QD/AuNP
CdSeTeS QD/AuNP with NoV-LPs (1 fg mL-1)
CdSe-TeS QD/AuNP with NoV-LPs (1 pg mL-1)
LSPR
Quenching
Fl intensity
Wavelength (nm)
(D)
Quenching CdSeTeS QD after AuNP addition
Enhancement after NoV-LPs addition
Fl Intensity
Size of AuNPs (nm)

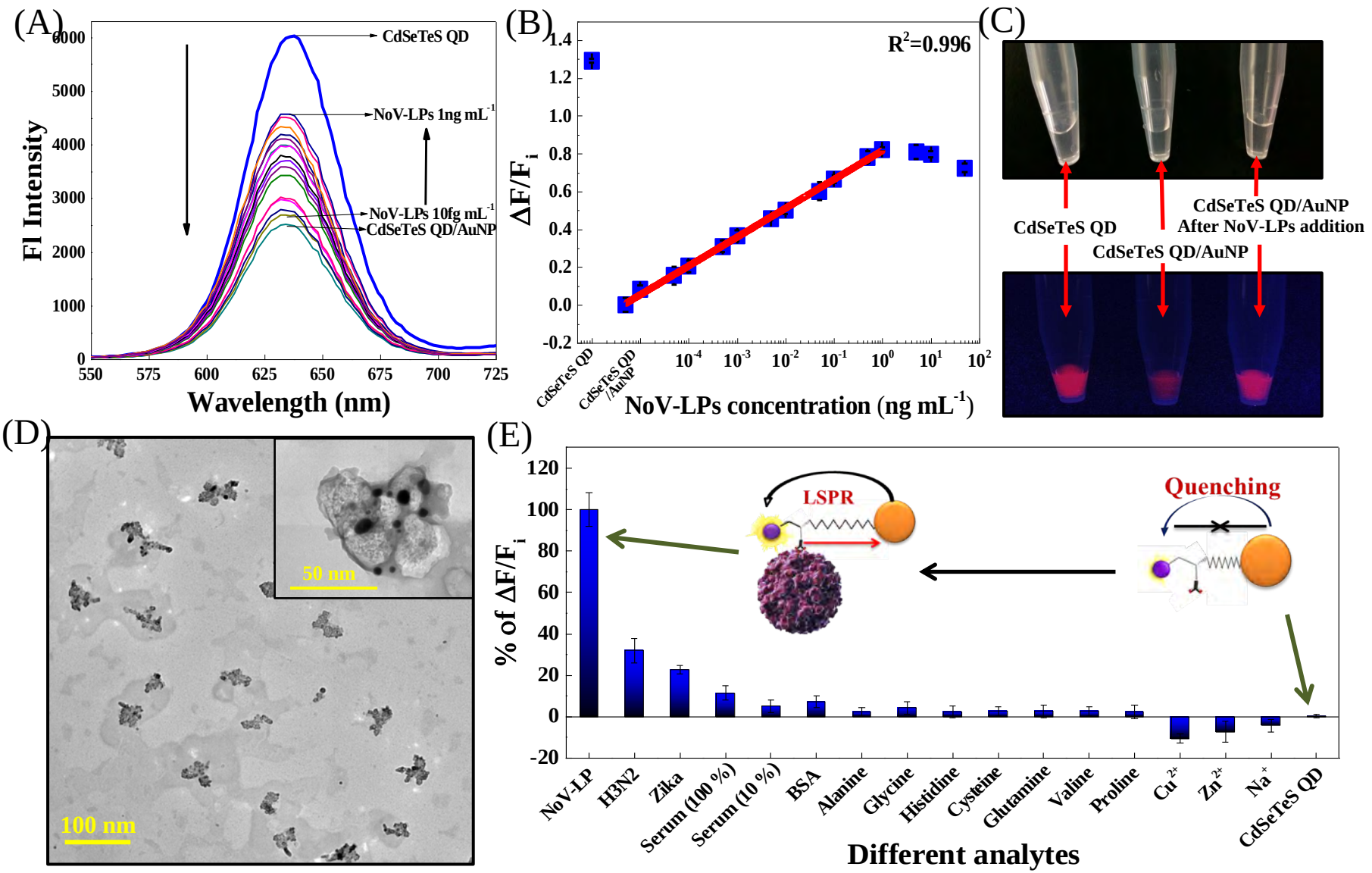
(A)
Fl Intensity
Wavelength (nm)
CdSeTeS QD
NoV-LPs 1ng mL-1
NoV-LPs 10fg mL-1
CdSeTeS QD/AuNP
(B)
R2=0.996
ΔF/Fi
NoV-LPs concentration (ng mL-1)
CdSeTeS QD
CdSeTeS QD /AuNP
(C)
CdSeTeS QD
CdSeTeS QD/AuNP
After NoV-LPs addition
CdSeTeS QD/AuNP
(D)
50 nm
100 nm
(E)
% of ΔF/Fi
LSPR
Quenching
NoV-LP
H3N2
Zika
Serum (100 %)
Serum (10 %)
BSA
Alanine
Glycine
Histidine
Cysteine
Glutamine
Valine
Proline
Cu2+
Zn2+
Na+
CdSeTeS QD
Different analytes

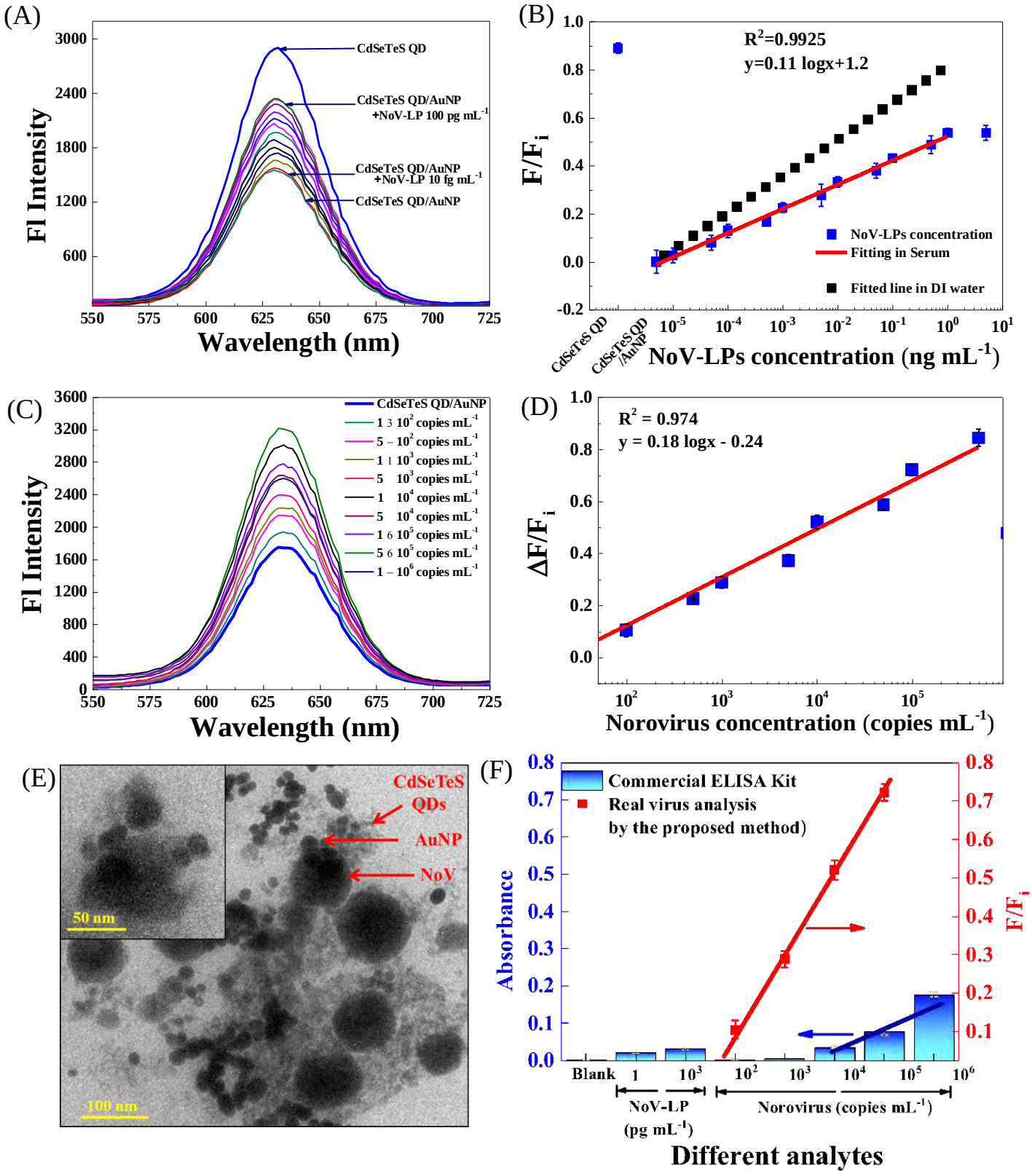
(A)
Fl Intensity
Wavelength (nm)
CdSeTeS QD
CdSeTeS QD/AuNP
+NoV-LP 100 pg mL-1
CdSeTeS QD/AuNP
+NoV-LP 10 fg mL-1
CdSeTeS QD/AuNP
(B)
R2=0.9925
y=0.11 logx+1.2
F/Fi
NoV-LPs concentration
Fitting in Serum
Fitted line in DI water
CdSeTeS QD
CdSeTeS QD /AuNP
NoV-LPs concentration (ng mL-1)
(C)
Fl Intensity
Wavelength (nm)
CdSeTeS QD/AuNP
1 3 102 copies mL-1
5 – 102 copies mL-1
1 1 103 copies mL-1
5 103 copies mL-1
1 104 copies mL-1
5 104 copies mL-1
1 6 105 copies mL-1
5 6 105 copies mL-1
1 – 106 copies mL-1
(D)
R2 = 0.974
y = 0.18 logx - 0.24
ΔF/Fi
Norovirus concentration (copies mL-1)
(E)
CdSeTeS QDs
AuNP
NoV
50 nm
100 nm
(F)
Commercial ELISA Kit
Real virus analysis
by the proposed method)
Absorbance
F/Fi
Blank
NoV-LP (pg mL-1)
Norovirus (copies mL-1)
Different analytes

Supplementary data

Single-step detection of norovirus tuning localized surface plasmon resonance-induced optical signal between gold nanoparticles and quantum dots

Fahmida Nasrin[a], Ankan Dutta Chowdhury[b], Kenshin Takemura[a], Jaewook Lee[b], Oluwasesan Adegoke[b], Vipin Kumar Deo[c], Fuyuki Abe[d], Tetsuro Suzuki[e], Enoch Y. Park[*,a,b]

[a] *Laboratory of Biotechnology, Graduate School of Science and Technology, Shizuoka University, 836 Ohya, Suruga-ku, Shizuoka 422-8529, Japan*

[b] *Laboratory of Biotechnology, Research Institute of Green Science and Technology, Shizuoka University, 836 Ohya, Suruga-ku, Shizuoka 422-8529, Japan*

[c] *Organization for International Collaboration, Shizuoka University, 836 Ohya, Suruga-ku, Shizuoka 422-8529, Japan*

[d] *Department of Microbiology, Shizuoka Institute of Environment and Hygiene, 4-27-2, Kita-ando, Aoi-ku, Shizuoka 420-8637, Japan*

[e] *Department of Infectious Diseases, Hamamatsu University School of Medicine, 1-20-1 Higashi-ku, Handa-yama, Hamamatsu 431-3192, Japan*

E-mails:

fnsoma@yahoo.com (FN)
dc_ankan@yahoo.co.in (ADC)
takemura.kenshin.16@shizuoka.ac.jp (KT)
lee.jaewook@shizuoka.ac.jp (JL)
adegoke.sesan@mailbox.co.za (OA)
deo.vipin.kumar@shizuoka.ac.jp (VKD)
fuyuki1_abe@pref.shizuoka.lg.jp (FA)
tesuzuki@hama-med.ac.jp (TS)
park.enoch@shizuoka.ac.jp (EYP)

[*] Corresponding author at: Research Institute of Green Science and Technology, Shizuoka University, 836 Ohya, Suruga-ku, Shizuoka 422-8529, Japan.
E-mail address: park.enoch@shizuoka.ac.jp (E.Y. Park). Tel (Fax): +81-54-238-4887)

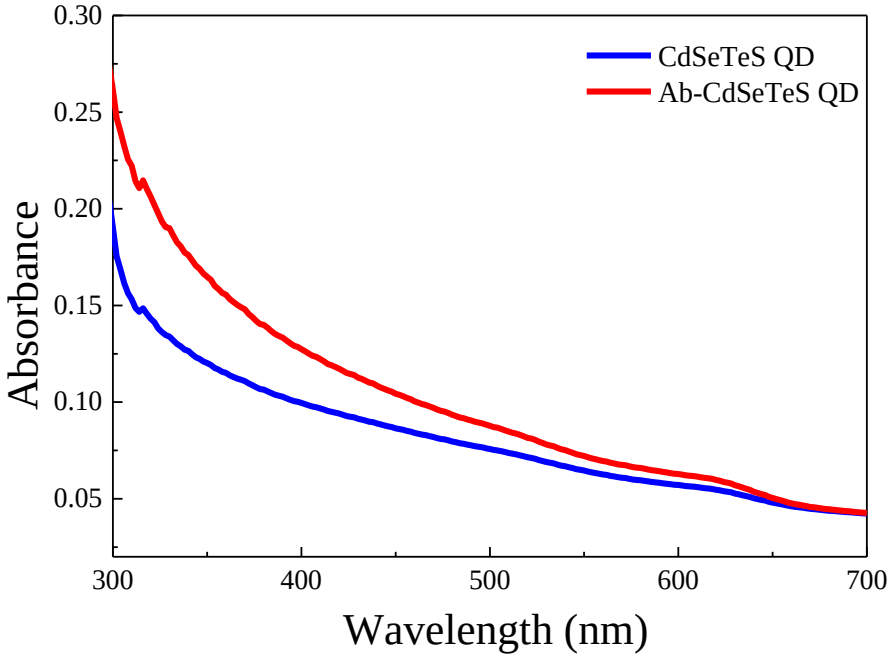

Fig. S1. UV-Vis spectra of CdSeTeS quantum dots before and after antibody conjugation.

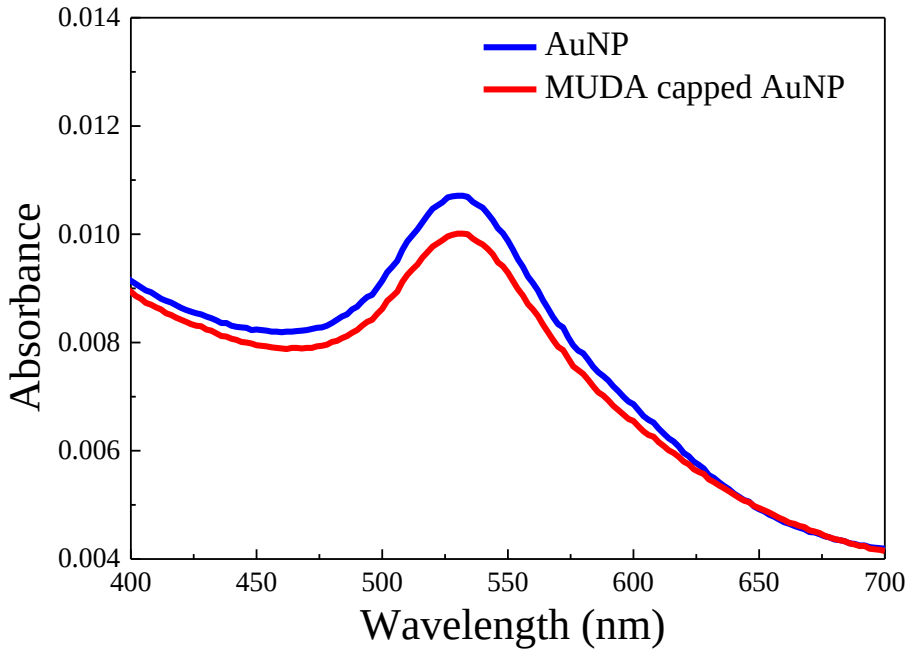

Fig. S2. UV-Vis spectra of AuNPs before and after capping with 11-mercaptoundecanoic acid.

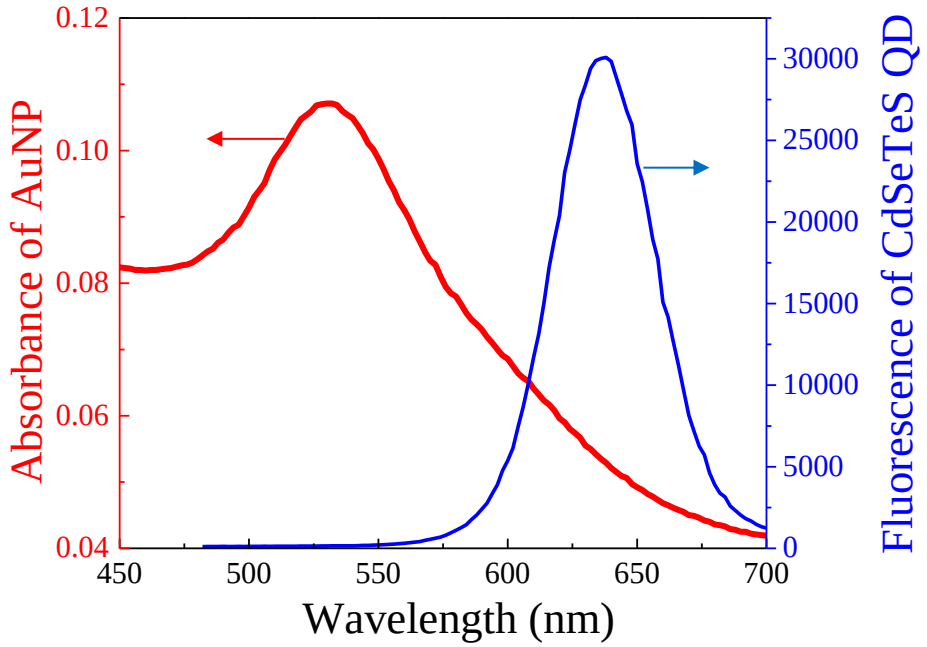

Fig. S3. The spectral overlap of SPR peak of AuNPs on CdSeTeS QDs emission spectra.

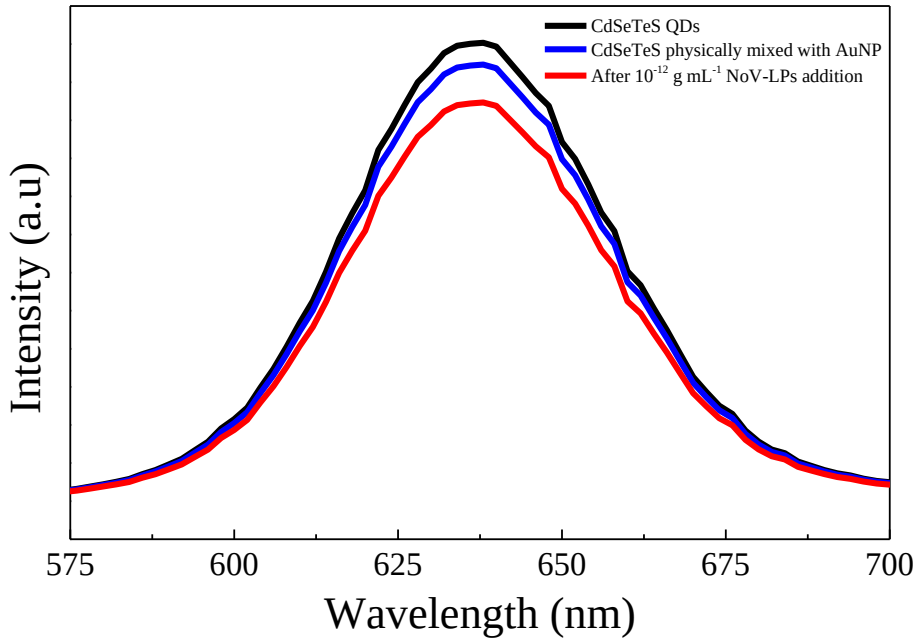

Fig. S4. Effect of non-covalently attached, physically mixed AuNPs on CdSeTeS QDs for NoV-LPs detection.

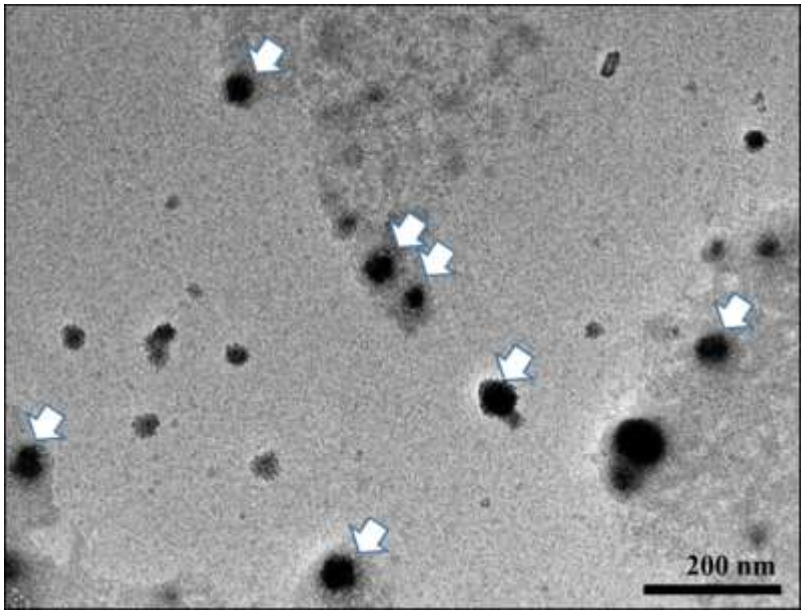

Fig. S5. TEM image of NoV-LPs. The VLPs (indicated by arrows) are in the range of 40–80 nm.